A 4.4-μW Wake-Up Receiver Using Ultrasound Data

Kshitij Yadav, *Student Member, IEEE*, Ioannis Kymissis, *Senior Member, IEEE*, and Peter R. Kinget, *Fellow, IEEE*

***Abstract*—In wireless sensor nodes, using a wake-up receiver to duty-cycle the main receiver significantly reduces the overall power consumption of the node, as long as the power consumption of the always-ON wake-up receiver is very low. We demonstrate line-of-sight ultrasound data communications for ultra-low power wireless wake-up in sensor networks. The 65-nm CMOS 0.6-V receiver prototype achieves a BER of better than 10^{-3} measured for a 250-bps free-space 8.6-m link in an indoor environment while dissipating only 4.4 μW and requiring only -18 dBm electrical power to be delivered to the transmit transducer.**

***Index Terms*—Node wake-up, ultrasound, wake-up receiver, wireless sensor nodes.**

I. Introduction

THE idea of ubiquitous embedded wireless sensor networks (WSNs) for environmental, industrial, and structural monitoring has been envisioned for over a decade. Progress has been made with advances in technology, but the realization of small autonomous nodes with long lifetimes remains an open challenge. Ubiquitous sensor networks consist of thousands of distributed nodes, which makes battery replacement both difficult and costly. This imposes very stringent constraints on the power budget of the accompanying hardware. Therefore, a key technological issue in making wireless sensor nodes widespread is the realization of node electronics with extremely low power consumption.

A sensor node has three primary functions: sensing, computation and communication. Out of these three functions, the communication circuitry consumes an overwhelmingly large percentage of the node energy [1]. However, the percentage of time during which the node has to communicate is small; this property of sensor nodes is exploited to reduce the power consumption of the node circuitry. The main transceiver is either duty-cycled and checks for communication requests periodically, or it is woken up only when a communication link has to be established with another node. The latter scheme requires an always-ON receiver called the wake-up receiver. The wake-up receiver turns on the main transceiver on the reception of a communication request from some other node in the network. For the current state-of-the-art RF receivers (Fig. 1(a)), the wake-up receiver's power consumption needs to be below about 50 μW for the wake-up approach to be more power efficient than the duty-cycled approach [2].

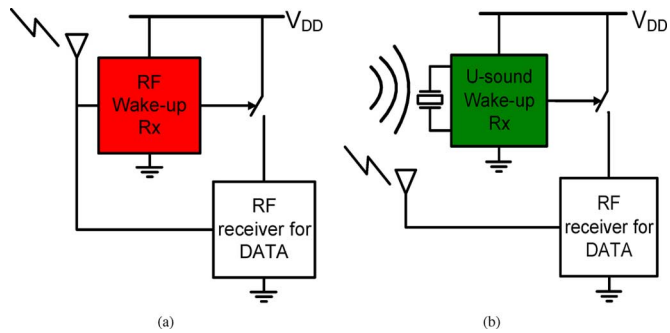

Fig. 1. (a) RF-based communication for both the main data and the wake-up receiver, and (b) proposed communication scheme that uses ultrasound for the wake-up and RF for the main-data communication.

The performance targets for the wake-up receiver and the duty-cycled main receiver are very different. The duty-cycled main receiver can receive a large number of bits in a relatively short time and then turn off; thus, its primary design target is low energy/bit. In contrast, the wake-up receiver is a 'wireless switch' that turns on the main receiver. Unlike the main receiver, the primary design target for the wake-up receiver is low continuous power consumption. The data-rate requirements in a wake-up receiver are more relaxed compared to a duty-cycled receiver [3]. In a duty-cycled receiver, a communication request from another node can only be received while the receiver is ON and each missed request has to be retransmitted; this increases the latency involved in establishing a communication link. In contrast, a wake-up receiver is always ON and a communication request from another node will be received at all times.

Low-power communication systems, using carriers different from the conventionally-used RF, have also been proposed. However, the requirements for the wake-up receiver in sensor networks are very different from what is available in these systems. Infra-red based communications have the potential to offer a low-power solution [4] but require accurate alignment of a narrow beam, which makes it less suitable for sensor-node applications.

In this paper, we have used ultrasonic data communications for wake-up [5]. Thanks to the much lower circuit speeds facilitated by using ultrasound carriers, the wake-up receiver in this work has one order-of-magnitude lower power consumption than the comparable low-power RF-based wake-up receivers [6], [7]. Further, owing to the short wavelength of ultrasonic waves (e.g., 8.5 mm @40 kHz), transducers with form factors of a few centimeters are possible even for frequencies as low as a few tens of kilohertz. Note that the addition of ultrasonic

Manuscript received June 11, 2012; revised September 09, 2012; accepted October 11, 2012. Date of publication January 28, 2013; date of current version February 20, 2013. This paper was approved by Associate Editor Eric A. M. Klumperink. This work was supported by the National Science Foundation with Grant ECCS-0925813.

The authors are with the Department of Electrical Engineering, Columbia University, New York, NY 10027 USA.

Color versions of one or more of the figures in this paper are available online at http://ieeexplore.ieee.org.

Digital Object Identifier 10.1109/JSSC.2012.2235671

wake-up to existing RF-based sensor nodes does not significantly increase the system cost, as the commercially available ultrasonic transducers are relatively inexpensive.

The low carrier frequencies of ultrasound limits the communication data rate and may contribute to wake-up latency [8]. However, for the targeted application of environmental and surveillance sensors, data rate requirements are fairly relaxed and the data rates offered by ultrasound suffice [9]. For some applications, the line-of-sight needed for ultrasound communication may limit the system performance. However, in many real-time equipment and personnel tracking applications [10], the confinement of ultrasound within the walls is actually a key advantage because it helps in achieving better tracking accuracy compared to RF-based systems.

Significant sources of strong ultrasonic interference are limited to environments with industrial manufacturing processes such as grinding, drilling, and fluid or air spray [11]. Based on our in-field measurements, the background noise in typical environments like homes and offices is much lower and does not significantly affects the performance of the ultrasound communication system. An exhaustive discussion on the effect of reflections and reverberation is beyond the scope of this paper but can be found in [12].

To the best of our knowledge, none of the existing ultrasound-based communication systems [10], [13] are suited for a low power application like the sensor node wake-up. In [13], a low-power detector for acoustic surveillance is proposed, but the sensitivity requirements for the acoustic receiver are much relaxed compared to what is needed for a wake-up receiver. Similarly, [10] uses ultrasound for real-time tracking. However, the receiver sensitivity is poor because the front end has been implemented by using an ADC only, without low-noise front-end amplifiers.

The remainder of the paper is organized as follows: in Section II, the electro-mechanical ultrasonic communication system is explained at the top-level and the mechanical part of the system, consisting of the ultrasound channel and the TX-RX transducer pair, is characterized to derive the performance requirements of the wake-up receiver chip. In Section III, circuit design of the wake-up receiver IC is explained. Section IV describes the electrical-only measurements of the wake-up receiver IC and the in-field measurements for a through-air wireless ultrasound data link in a lecture hall. The paper ends with the concluding remarks offered in Section VI.

II. System Level Considerations

A. Using Different Communication Media for the Wake-Up and the Main Data

We propose a communication scheme where ultrasound is used for wirelessly waking up sensor nodes (Fig. 1(b)), while the RF is used to communicate the main data. This scheme exploits extremely low-power, but lower data rate, ultrasonic communications to realize a 'wireless switch' that turns ON a more power consuming, but higher data rate, RF transceiver to carry out the main data communication.

B. Regulations on Ultrasonic Transmissions

We could not find any legally enforceable limits on the through-air transmission of ultrasound. Ultrasound is in general considered safe for the human body. For this reason, the ultrasound emission limits recommended by various government and non-government organizations are relatively relaxed. For diagnostic ultrasound, the Food and Drug Administration (FDA) recommends ultrasound pressure levels to be below 620 Pa [14]. The Occupational Safety and Health Administration (OSHA) imposes limits for frequencies below 8 kHz [15], but there are no limits on ultrasonic frequencies. The American Conference of Governmental Industrial Hygienists (ACGIH) recommends pressure levels below 355 Pa for ultrasound [16]. Most of the recommendations discussed above are for applications that are very different from wireless data communication, but they still give an idea of the relative safety of ultrasound. In our field measurements, for a communication distance range of 8.6 m, pressure at a distance of 0.305 m (1 foot) from the transmitter is only 0.2 Pa. Thus, the transmitted pressure levels in this work are more than four orders of magnitude below the recommendations and their transmission in real environments will not pose any problem.

C. The Ultrasound Data Communication System

Fig. 2 shows a block-level diagram of the through-air ultrasound data communication system. We have used ON-OFF Keying (OOK) modulation because it enables the use of simple energy detection receivers; these receivers are an attractive choice for a power constrained application [6] like wake-up because they don't need a frequency synthesizer for the LO generation and can thus be realized with ultra-low power consumption. At the transmitter, an OOK electrical signal is generated by mixing the data bits with a 40.6-kHz sine-wave carrier. The electrical signal excites the transmit transducer, which produces modulated ultrasonic pressure waves. These pressure waves travel through air and suffer path loss before reaching the receiver, where they are converted into an electrical signal by the receive transducer. The wake-up receiver IC is designed for ultra-low power consumption, and extracts the transmitted bits from the received electrical signal such that the required bit error ratio (BER) are achieved for the targeted communication distances.

D. Receive and Transmit Ultrasonic Transducers

The envisioned application environment for this work consists of a one-way wake-up link between the ultrasonic transmitter at the base station and an ultrasonic receiver in each network node. The transmit and the receive transducers have different sets of requirements. The base station transmit transducer must have a high transmit efficiency, while the form factor is not a primary criterion. On the other hand, the receive transducers are being used at the network nodes and must have a small form-factor for them to work unobtrusively within the physical environment. The ultrasonic transducers used in this work are made of piezoelectric materials that have the property of converting electrical energy into mechanical energy and vice-versa.

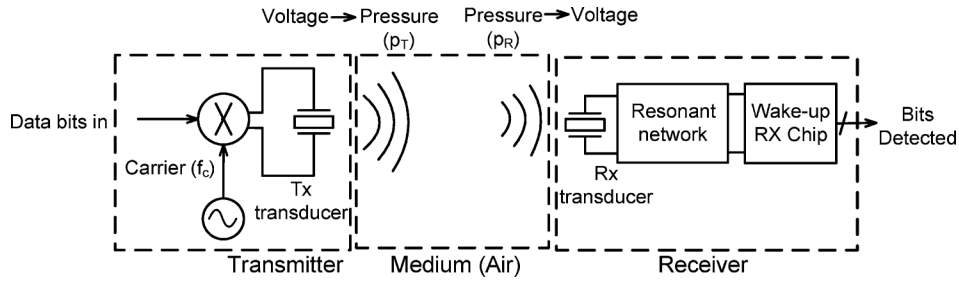

Fig. 2. Block diagram of the ultrasound data communication system.

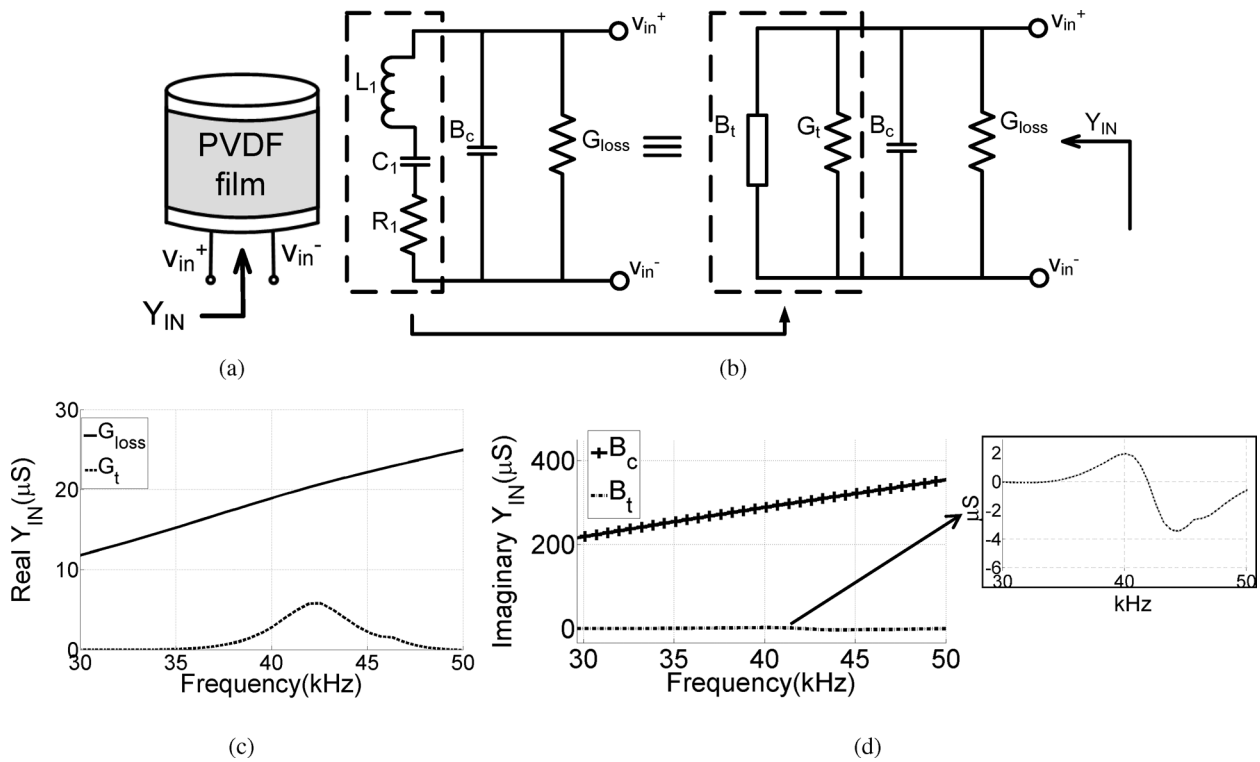

Fig. 3. (a) Structure of the piezoelectric receive transducer, (b) the equivalent circuit, (c) the measured real admittance, and (d) the measured imaginary admittance.

At the transmitter, a highly efficient metal-piezoelectric unimorph [17] is used. The unimorph is cylindrical in shape, and has a diameter of 2.5 cm and a height of 1.2 cm. This class of transducers exploits the difference between the piezoelectric constants of Aluminum and PZT (Lead Zirconate Titanate) to enhance the efficiency of ultrasound transmission. These transducers are directional; however, several transducers can be easily combined to achieve omnidirectional transmission.

The receive transducer [18] consists of a piezoelectric film (Fig. 3(a)), Polyvinylidene Fluoride (PVDF), wrapped around a hollow plastic cylinder that has a diameter of 1.5 cm and a height of 2.6 cm. To match the output impedance of this transducer with the receiver input, we study the input admittance of the transducer, Y_{IN}. It consists of a capacitive part because of piezoelectric film capacitance $(\mathrm{B_c})$, a resistive part because of dielectric loss $(\mathrm{G_{loss}})$, and a series LCR circuit to model the electrical equivalent of the transducer's mechanical resonance (Fig. 3(b)) [19]. The real and the imaginary parts of the measured admittance are shown in Fig. 3(c) and (d). While the real part is dominated by the dielectric loss G_{loss}, a contribution from the transducer action G_{t} is also observed: $R_1/(R_1^2 + (\omega L_1 - 1/(\omega C_1))^2)$; a peaking is observed in $\mathrm{G_t}$ at the mechanical resonance frequency of the transducer at 40 kHz. The imaginary part is dominated by $\mathrm{B_c}$, but also has a contribution from the transducer action, $\mathrm{B_t} = -(\omega L_1 - 1/(\omega C_1))/(R_1^2 + (\omega L_1 - 1/(\omega C_1))^2)$. The inset in Fig. 3(d) shows $\mathrm{B_t}$ which has a zero-crossing at the mechanical resonance frequency. As can be seen from the discussion above, the input admittance of the transducer is dominated by the film capacitance and the dielectric loss; the contributions from the transducer action dwarf in comparison. Thus, while choosing the first-stage amplifier topology, we use the transducer model shown in Fig. 4(a). The electrical signal induced because of piezoelectricity is modeled as a current source in parallel with the transducer input admittance.

E. First-Stage Amplifier and the Receive Transducer

The first-stage amplifier determines the noise performance of the receiver. With the given receive transducer,

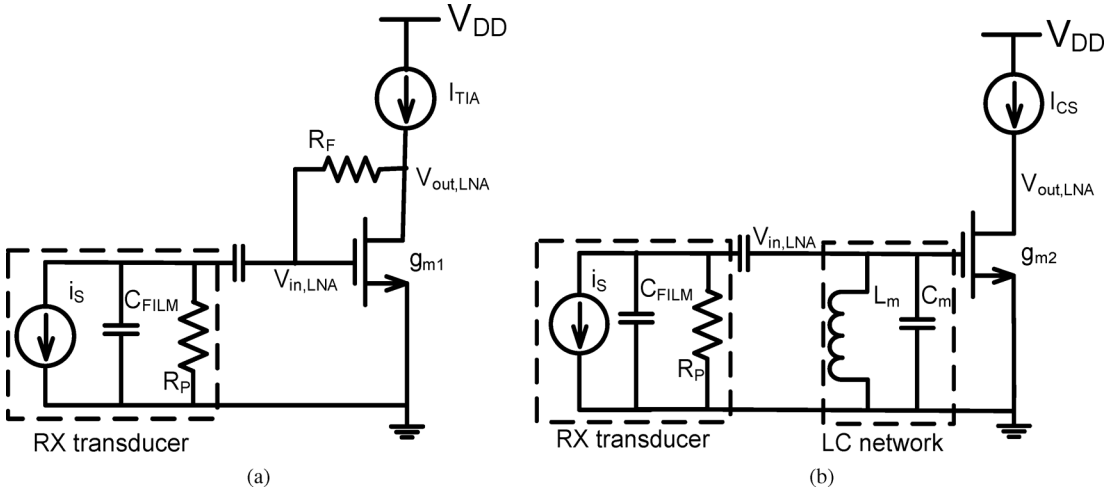

Fig. 4. Candidate topologies for the low noise amplifier: (a) a transimpedance amplifier, and (b) a common-source amplifier with LC resonance peaking circuit.

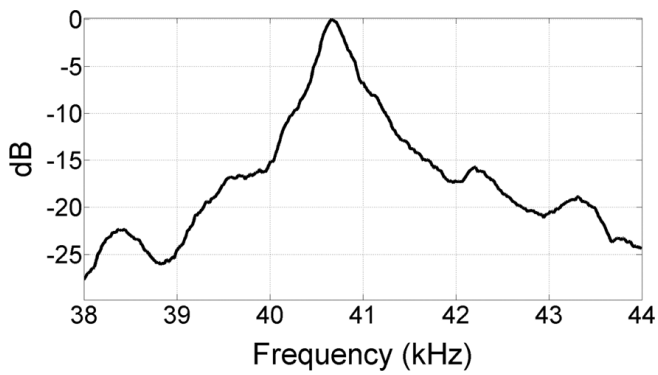

Fig. 5. Measured transmission characteristics vs. frequency of the TX-RX ultrasound transducer pair.

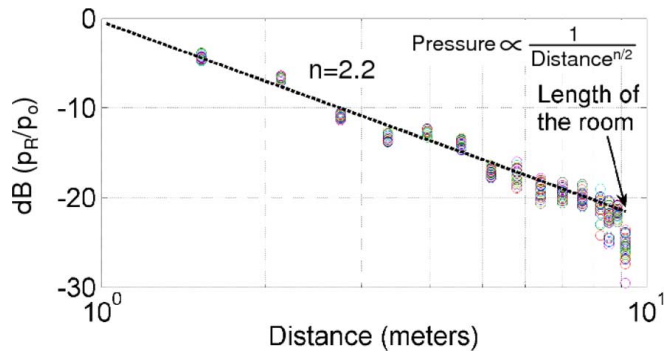

Fig. 6. Received pressure (p_R) (normalized for a TX-RX distance of 1 m) vs. TX-RX distance inside a lecture hall, measured using a reference acoustic pressure measurement system [21].

several first-stage topologies were considered for best possible noise performance. Two prominent ones are the TIA (Trans-Impedance Amplifier) and the common-source amplifier with a resonance peaking circuit. A TIA is often used with transducers whose output signal is a current [20]. The input impedance of the TIA ($1/g_m$ in Fig. 4(a)) must be much lower than the transducer output impedance $(1/(\omega C_{\mathrm{FILM}}))$; otherwise the AC current signal from the transducer is lost in C_{FILM}, resulting in a poor signal-to-noise ratio at the output. This imposes a limit on the minimum value of the transistor transconductance and hence a limit on the minimum current consumption of the circuit. For the receive transducer used in this research, assuming a g_m/I of 30, we would need $I_{\mathrm{TIA}} \gg 10\ \mu$A, which is too high for the power-consumption levels targeted in this research. In comparison, common-source amplifier with a resonance peaking circuit (Fig. 4(b)) meets the performance requirements with lower current consumption because of voltage peaking of the received signal by the LC tank, which was used to match the transducer's output admittance. Therefore, in this work, we have used this circuit to realize the first stage of the receiver; the surface-mounted tank ($\mathrm{L_m} = 10$ mH, $\mathrm{C_m} = 0.41$ nF) resonates with the transducer film capacitance ($C_{\mathrm{FILM}} = 1.14$ nF) at 40 kHz. The resonance peaking network and the transducer combination has an electrical quality factor (Q) of 14 and a parallel resonant impedance $(R_p \| R_{\mathrm{LC}})$ of 36.3 kΩ.

F. Link Budget

In this section, the transmission characteristics of the TX-RX transducer pair are combined with the pressure vs. distance measurements done in a lecture hall, to derive the sensitivity requirements of the ultrasonic receiver IC; the specifications have been derived for a communication distance range of 8 m, the length of a typical lecture hall.

The bandwidth and the insertion loss of the TX-RX transducer pair are measured by sweeping the electrical excitation to the TX across frequency and then observing the open-circuit voltage across the RX transducer (Fig. 5). The bandwidth of the transducer pair is 300 Hz and is determined by the high Q (>100) of the transmit transducer, which limits the communication data rate; in comparison, the bandwidth of the receiver electronics is 2 kHz. The insertion loss of the pair at the resonance frequency of 40.6 kHz is 61 dB for a TX-RX distance of 1 foot (0.305 m). A relatively high value of the insertion loss is because of the inherently low electro-mechanical conversion efficiency ($\mathrm{k_5^2}$ = Fraction of applied electrical energy converted into mechanical energy) of the piezoelectric materials—for PZT

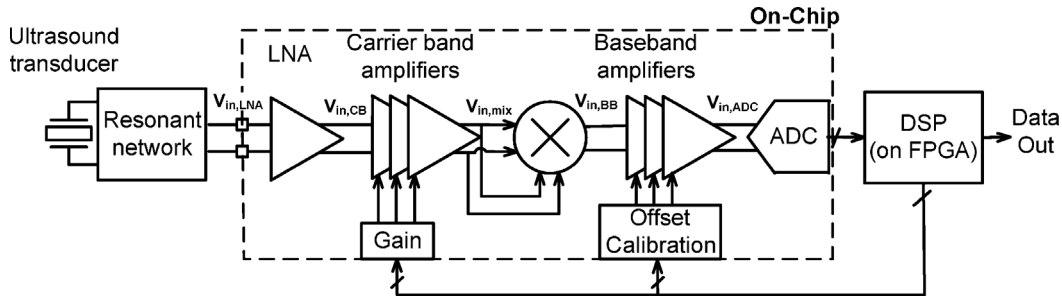

Fig. 7. Block diagram of the ultrasound wake-up receiver.

(transmit transducer), k_5^2 is 0.15, while for the PVDF (receive transducer), k_5^2 is 0.025 [19].

Pressure vs. distance measurements (Fig. 6) were done in a lecture hall in the presence of typical interferers and reverberations by using a reference acoustic pressure measurement system [21]. The pressure is observed to be inversely proportional to distance—$\text{Pressure} \propto 1/\text{Distance}^{(n)/(2)}$—with an exponent n of around 2.2[1]. The measured value of n is greater than 2, the value for a spherical wave front [22], because of the effect of reverberations and multi-path.

Insertion loss at the targeted communication distance range of 8 m is calculated by using the formula:

$$IL(d) = IL(0.305\text{m}) + n10\log_{10}\left(\frac{d}{0.305\text{m}}\right) \qquad (1)$$

where $IL(d)$ is the insertion loss in dB and d is the TX-RX distance in meters. Using an exponent n of 2.2, as derived from the pressure vs. distance measurements (Fig. 6), the insertion loss is calculated to be 92.2 dB at 8 m.

In this work, we are targeting an order-of-magnitude reduction in both the transmit power and the receiver power consumption. Comparable RF-based wake-up receivers [6], [7] use a transmit power of around 1 mW; here, the electrical power delivered to the transmitter transducer is only 16 μW. For the transmit transducer used in this research, this corresponds to an excitation of 70.7 mV_{rms}; for this excitation, the open-circuit voltage at the receive transducer at a distance of 8 m is 1.73 μV_{rms}. Since we are using an LC tank at the receiver, the voltage at the input of the receiver IC ($v_{\text{in,LNA}}$) peaks at the resonance frequency by a factor of $R_p \| R_{\text{LC}}/(1/\omega C_{\text{FILM}})$, to 18.3 μV_{rms}. Thus, we target a receiver voltage sensitivity (S_{in}) of around 18 μV_{rms}.

The voltage noise squared density at the input of the receiver because of the resonance peaking network and the transducer combination is $4kT(R_p \| R_{\text{LC}})$. Thus, the signal-to-noise ratio (SNR_{in}) at the receiver input, for the 2-kHz bandwidth (BW_t) of the combination and for an input voltage around the sensitivity level, is given by $(S_{\text{in}}^2)/((4kTR_p \| R_{\text{LC}})\text{BW}_t)$, which is around 24.5 dB. For the OOK-based energy-detection receiver used in this research, a SNR_{out} of around 10 dB is needed to achieve a BER of better than 10^{-3}. Thus, the noise figure[2] specification (NF_{RX}) for the receiver is 14.5 dB ($= \text{SNR}_{\text{in}} - \text{SNR}_{\text{out}}$). Even though the noise performance of the OOK-based energy detection receivers is poorer as compared to their coherent counterparts, a NF_{RX} of 14.5 dB is achievable while maintaining an ultra-low power dissipation.

[1]Note that the more widely used power-distance exponent for this system is twice of the pressure-distance exponent because mechanical power is proportional to pressure^2; hence, $(n)/(2)$ in the exponent.

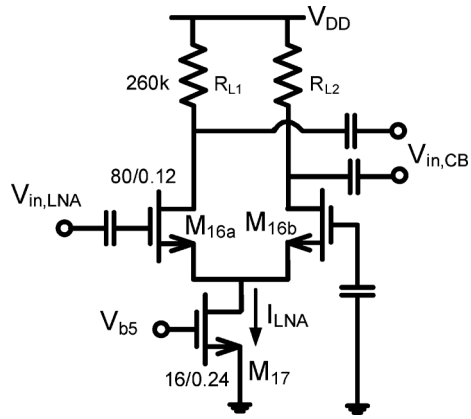

Fig. 8. Low noise amplifier circuit. Device sizes (W/L) are in the units of μm/μm and devices in symmetrical paths have the same sizes. DC biasing is not shown.

III. Ultrasonic Wake-Up Receiver IC Design

The ultra-low power OOK-based energy-detection receiver (Fig. 7) in this work uses self-mixing for signal downconversion. To achieve good dynamic range and to realize a receiver with a sensitivity level of a few tens of μV, the LNA is followed by a cascade of amplifiers. The downconversion is realized by using a Gilbert-cell based self mixer. The down-converted baseband signal is then amplified, using op-amp based resistive-feedback amplifiers, to fully utilize the dynamic range of the 5-bit successive approximation register (SAR) analog-to-digital converter (ADC).

A. Low Noise Amplifier Design

The first stage is realized by using a simple differential amplifier (Fig. 8). Instead of an active PMOS load, a resistive load has been used. Despite a lower voltage gain, the resistive load offers better receiver noise performance, thanks to the lower noise of the resistors. In cascaded amplifiers, the noise of the first stage contributes directly to degradation of the signal-to-noise ratio.

[2]Strictly speaking, noise figure is defined only for linear systems. But, for simplicity and intuition, we have used this nomenclature here [6].

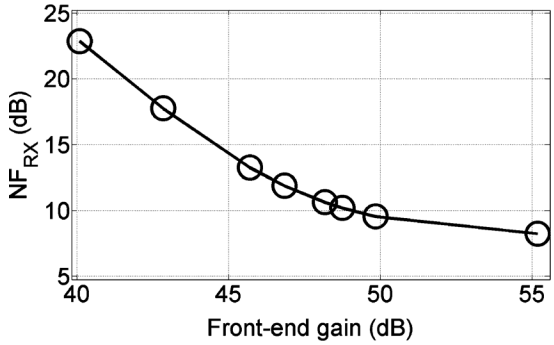

Fig. 9. Receiver noise figure ($\mathrm{SNR_{in,LNA}} - \mathrm{SNR_{in,ADC}}$) vs. front-end gain ($v_{\mathrm{in,mix}}/v_{\mathrm{in,LNA}}$) for an input signal ($v_{\mathrm{in,LNA}}$) of 40 $\mu\mathrm{V_{rms}}$.

To keep its noise contribution sufficiently low, the first stage is designed to consume as much as 40 percent of the overall analog receiver power; the tail current, I_{LNA}, is 2.7 μA. The ultrasound carrier frequencies of 40 kHz are very low compared to the intrinsic device speeds in 65-nm CMOS and devices can be operated deeply into weak inversion to achieve maximum current efficiency ($g_m/I = 31$) to keep the thermal noise low. However, careful attention must be paid to keep the flicker noise low; for this reason, large NMOS devices are used in the carrier-band amplifiers. The first-stage differential NMOS devices ($\mathrm{M_{16a}}, \mathrm{M_{16b}}$) were sized 80 μm/0.12 μm, thus keeping the flicker noise corner (f_c) to 6 kHz, well below the carrier frequency of 40 kHz. Load resistors ($\mathrm{R_{L1}}, \mathrm{R_{L2}}$) of 260 k$\Omega$ have been used; a higher value will give more gain, but the maximum usable resistance value is limited by the tight voltage headroom in this low-voltage (0.6 V) design. The stage has a voltage gain ($v_{\mathrm{in,CB}}/v_{\mathrm{in,LNA}}$) of 14.7 dB and has a noise figure ($\mathrm{SNR_{in,LNA}} - \mathrm{SNR_{in,CB}}$) of 6.15 dB.

B. Carrier-Band Amplifiers

The gain in the carrier-band ($A_v = v_{\mathrm{in,mix}}/v_{\mathrm{in,LNA}}$) must be sufficiently high to suppress the noise contribution from the baseband amplifiers. To analyze the effect of front-end gain on the receiver noise figure ($\mathrm{NF_{RX}}$),[3] a verilogA model of the receiver was developed, taking into account the noise contribution of each stage, both the thermal noise and the flicker noise. A cascade of four amplifiers succeeds the first-stage LNA; the first and the last stage amplifiers are fixed-gain, while the other two amplifiers are gain-tunable. For an input signal level ($v_{\mathrm{in,LNA}}$) of around 40 $\mu\mathrm{V_{rms}}$ and A_v less than about 40 dB, the receiver output noise is dominated by the flicker noise of the baseband-amplifiers, and varies as 20 dB per decade of A_v (Fig. 9) because of the squaring action of the self-mixer. However, for larger values of A_v (>48 dB), the noise contributions from the LNA and the second-stage amplifier dominate the receiver output noise; any increase in the front-end gain beyond this point does not improves the receiver performance appreciably. Keeping some margin, the receiver presented in this work has been designed for a maximum front-end gain of 55 dB.

For the fixed gain stages, we have used NMOS differential amplifiers with PMOS loads; the amplifiers are accompanied by CMFB circuits (Fig. 10). The input device pairs (M_{6A}, M_{6B}) were sized at 200 μm/0.12 μm and operate in weak inversion with a g_m/I of 32. Current levels have been kept low at a few 100 nA, resulting in a high small-signal output resistance, $r_o = V_A/I$. For a typical early voltage of around 1 V, r_o is around 10 MΩ for a 0.12-μm device. These high output resistances in combination with the capacitive input impedance (around 300fF, dominated by miller capacitance due to C_{gd}) of the next stage would however result in poles around 50 kHz, which is too close to the ultrasonic carrier frequencies. Therefore, differential amplifiers with NMOS diode-connected loads have to be used as buffers to connect the amplifier outputs to the input of the next stage. The first and the last PMOS-load stages have gains of 16.5 dB and 11.2 dB.

The two VGAs are identical and are made using NMOS differential amplifiers with diode-connected PMOS load (Fig. 11). Connected in parallel with the diode-connected PMOS load are the PMOS-based switched-current sources ($I_{\mathrm{VGA},1}$, $I_{\mathrm{VGA},2}$), which are used to control the current through the PMOS load and thereby tune the amplifier gains (g_{mn}/g_{mp}). The tail currents ($I_{\mathrm{VGA,tail}}$) for the two VGAs are 139 nA and 147 nA. For both the VGAs, $I_{\mathrm{VGA},1}$ and $I_{\mathrm{VGA},2}$ are 25 nA and 33 nA, giving gain tunability (using g[0:1] and g[2:3]) from 0 dB to 14.4 dB and 0 dB to 10.2 dB. Operation in weak inversion ensures a high g_m/I of 31. The simulated overall noise figure ($\mathrm{SNR_{in,CB}}$–$\mathrm{SNR_{in,mix}}$) of the carrier-band amplifiers is 2.5 dB.

C. Base-Band Amplifiers, Self-Mixer and 5-Bit SAR ADC

The envelope of the carrier-band signal is demodulated by using a Gilbert-cell based self-mixer (Fig. 12) that outputs a current signal into a transimpedance amplifier, which is realized with resistive feedbacks around an OTA. In this work, all the transistors are operating in weak inversion and the current is given by $I = I_s \exp((V_{\mathrm{GS}})/(nkT/q))$ when the drain voltage, $V_D \gg kT/q$ and the source-bulk voltage, $V_{\mathrm{SB}} = 0$. The differential output current ($i_{\mathrm{out,BB1^+}} - i_{\mathrm{out,BB1^-}}$) of the mixer is

$$i_{\mathrm{out,BB}} = I_{\mathrm{BIAS,mix}} \frac{\left(\exp\left(\frac{v_{\mathrm{in,mix}}}{2nkT/q}\right) - \exp\left(\frac{-v_{\mathrm{in,mix}}}{2nkT/q}\right)\right)^2}{\exp\left(\frac{v_{\mathrm{in,mix}}}{2nkT/q}\right) + \exp\left(\frac{-v_{\mathrm{in,mix}}}{2nkT/q}\right)} \tag{2}$$

where $I_{\mathrm{BIAS,mix}}$ is the tail current as shown in figure, $v_{\mathrm{in,mix}}$ is the input signal and n is the sub-threshold slope factor. For smaller input signals ($v_{\mathrm{in,mix}} \ll 2\sqrt{3}nkT/q \approx 120$ mV @300 K)[4], the expression reduces to:

$$i_{\mathrm{out,BB}} = 2I_{\mathrm{BIAS,mix}} \left(\frac{v_{\mathrm{in,mix}}}{2nkT/q}\right)^2 = a_2 v_{\mathrm{in,mix}}^2 \tag{3}$$

Thus, the squared conversion gain, a_2, is proportional to the bias current. In this work, we have used $I_{\mathrm{BIAS,mix}} = 29$ nA, giving a simulated a_2 of 12 $\mu\mathrm{A/V^2}$. A higher mixer conversion gain could be achieved by using a larger mixer bias current; instead we achieve a high receiver gain by designing the 40 kHz front-end for high gain. This technique is more efficient because unlike RF-based receivers, where front-end gain comes at the

[3]A mathematical model has been used to speed up the simulation times. Results from the model were verified to match closely with the transistor-level simulations.

[4]For an input voltage at the targeted sensitivity level, $v_{\mathrm{in,mix}} = 29\mathrm{mV}_{p-p}$; thus, the simplifying assumption.

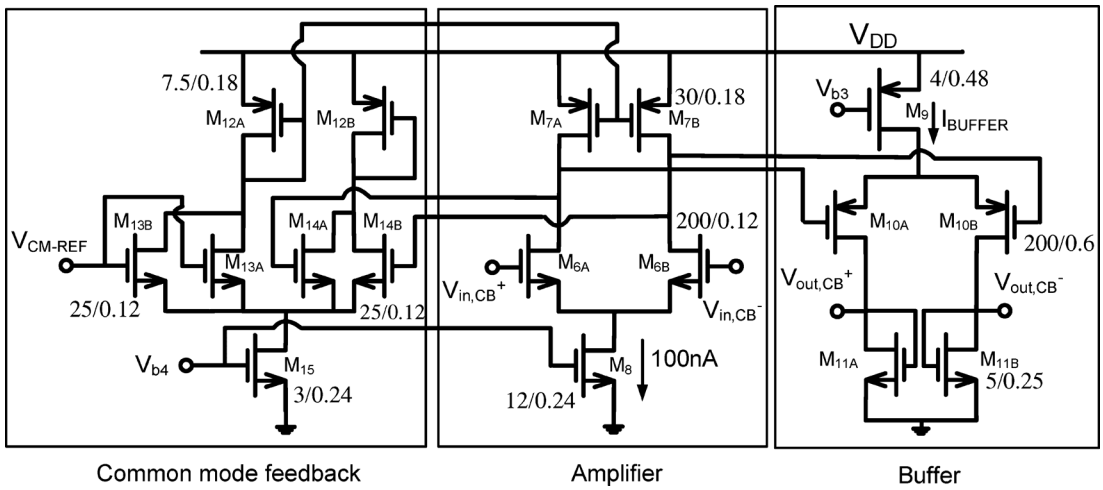

Fig. 10. Carrier-band amplifier circuit. Device sizes (W/L) are in the units of μm/μm and devices in symmetrical paths have the same sizes. DC biasing is not shown.

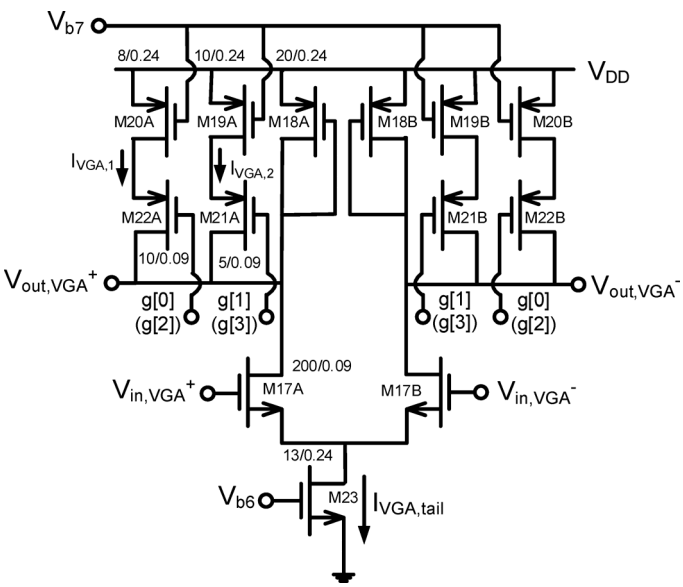

Fig. 11. Variable-gain amplifier circuit. Bits g[0:1] (g(2:3)) are used to control the first (second) VGA. Device sizes (W/L) at in the units of μm/μm and devices in symmetrical paths have the same sizes. DC biasing is not shown.

cost of power-hungry gigahertz amplifiers, any additional gain in the ultrasonic front-end can be realized with a power consumption of just a few tens of nanoamperes.

The output of the baseband must be within the dynamic range of the ADC and therefore has to be amplified further. For an input signal $(v_{\mathrm{in,LNA}})$ at the targeted receiver sensitivity, the output of the TIA $(V_{\mathrm{in,BB1}})$ is 1.2 mV_{p-p} (Fig. 13). This is well below the 19 mV resolution of the 0.6-V 5-bit ADC, which succeeds the baseband amplifiers. Thus, we amplify the signal by 30 dB using a cascade of two OTA-based resistive-feedback amplifiers. The OTAs are fully-differential two-stage amplifiers, consisting of a differential amplifier with PMOS load and a CMFB circuit, followed by a common-source amplifier stage. The OTAs have to work at low frequencies of a few kilohertz; thus, to keep the 1/f flicker noise low, NMOS devices at OTA inputs are sized large, 50 μm/0.24 μm. The power consumption of the base-band amplifiers is limited by the current that the OTAs have to drive into the resistive loads to achieve the required voltage swing. To keep this current below a few hundred nanoamperes, while achieving an output voltage swing of a few tens of mVs, resistors in the order of MΩs have been used. These large resistors are realized by using poly resistors having a density of 5.5 $\mathrm{k}\Omega/\mu\mathrm{m}^2$. Using even larger resistors would decrease the power consumption of the OTAs, however this comes at the cost of a substantial increase in area.

A DC-offset cancellation mechanism has been implemented to cancel the offsets due to self-mixing and device mismatch. Switched resistors, of the order of a several MΩs, have been used to inject differential currents into the feedback resistors. Poly resistances of a total value of 100 MΩ and occupying a total area of 500 μm $\times$ 100 μm have been used. Though the resistor area could have been reduced by using MOSFET resistances, poly resistors have been used to keep the flicker noise low.

The analog receiver output $(v_{\mathrm{in,ADC}})$ is converted into a 5-bit digital word using a fully-differential SAR ADC. The anti-aliasing filter is implemented by using a first-order RC filter in the last-stage baseband amplifier. A capacitive DAC [23], as opposed to a resistive DAC, has been used so that the same circuit can be used both as a DAC and as a sampling circuit; another benefit of using capacitive DACs is that they do not suffer from any static power consumption. A sampling rate of 2 kS/s was used for over-sampling the data by eight times; the ADC power consumption at this sampling rate was measured to be 400 nW.

D. Digital Back-End

In order to estimate the power consumption of the digital back-end, threshold recovery, majority bit-decision, digital early-late clock recovery [24] and DC-offset calibration (Fig. 14) were implemented on a Cyclone II FPGA using VHSIC Hardware Description Language (VHDL). Based on the number of combinational functions and logic registers occupied on the FPGA, the number of transistors for an ASIC

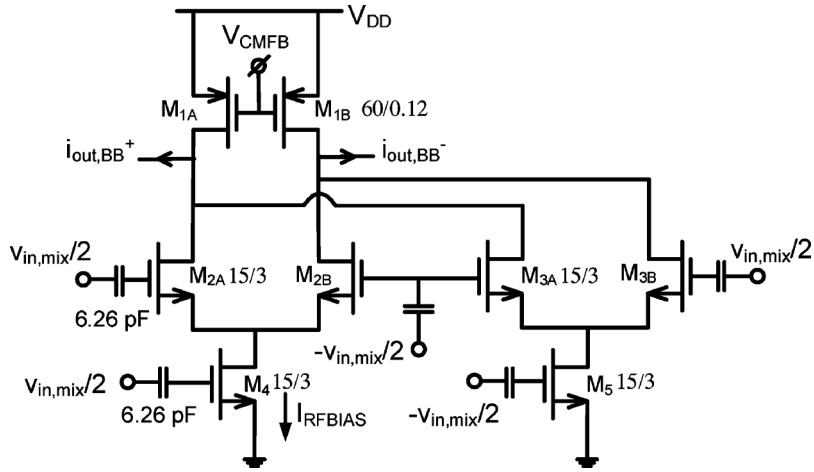

Fig. 12. Gilbert-cell based self-mixer. Device sizes (W/L) are in the units of μm/μm and devices in symmetrical paths have the same sizes. DC biasing is not shown.

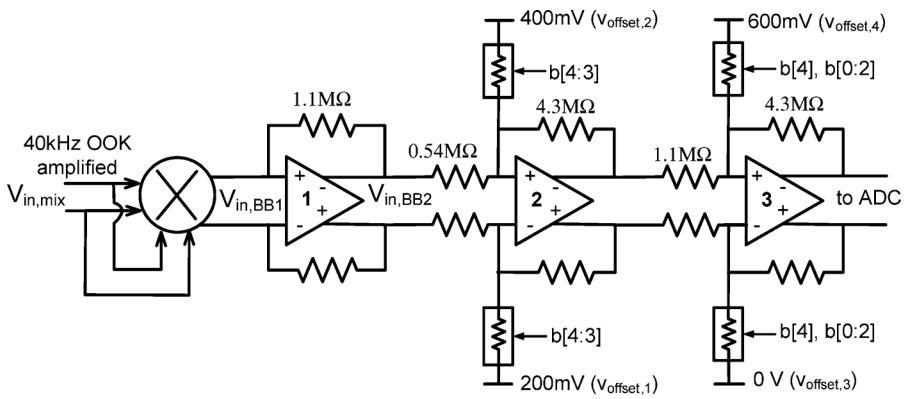

Fig. 13. Op-amp based resistive feedback amplifers in the base-band.

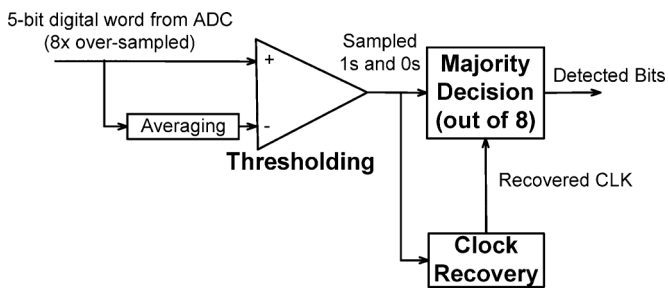

Fig. 14. Block-level diagram of the digital back-end.

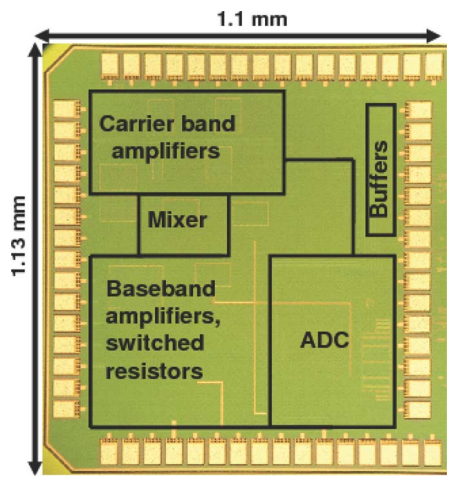

Fig. 15. Receiver die photo in 65 nm CMOS.

implementation was estimated to be 107k [25]. For a 65-nm CMOS process, assuming minimum sized two-input gates (Total Width $= 0.7$ μm, Length $= 65$ nm), plus an activity factor of unity and a clock frequency of 2 kHz (ADC sampling clock), the power consumption of the digital back-end circuit is estimated to be 15 nW.

For this work, a crystal oscillator on a commercial FPGA board was used for clock generation. In a full implementation, an ultra-low-power 32 kHz crystal oscillator (e.g., Micro Crystal's OV-7604-C7, which can operate at 360 nW) may be used. Therefore, the overall power consumption at the receiver is estimated to be $4.4\mu\text{W} + 360\ \text{nW} + 15\ \text{nW} = 4.78\ \mu\text{W}$; it is dominated by the analog front-end IC which we have built and have shown to be able to function at low power. The power consumptions of the digital back end and the clock generator are negligible in comparison.

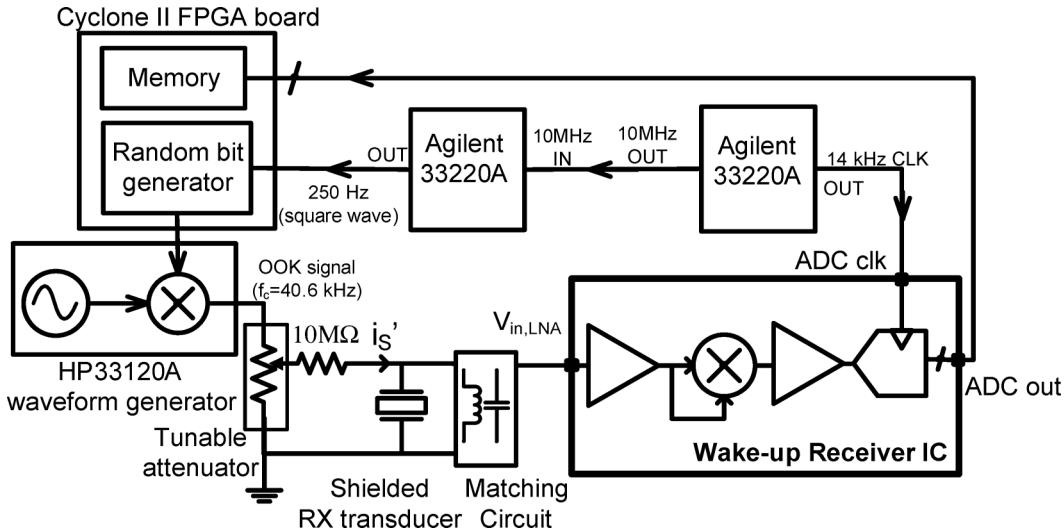

Fig. 16. Testbench for the electrical-only BER measurements.

IV. Experimental Results

The chip photograph is shown in Fig. 15. The receiver was fabricated in a 65-nm CMOS process and occupies a silicon area of 1.24 mm^2.

A. Electrical-Only Measurements

Fig. 16 shows the testbench used for electrical-only BER characterization of the wake-up receiver IC. To mimic the current signal (i_s') as will be generated by the transducer during field measurements, a 10 MΩ resistor was used in series with an OOK voltage signal obtained by mixing pseudo-random bits from the FPGA and a 40.6 kHz sine-wave carrier. A shielded transducer was used in parallel with the resonance peaking circuit to obtain impedance levels similar to those in the field measurements. The 250 Hz data clock and the 14 kHz ADC sampling clock were generated using waveform generators and were synchronized using an external loop, though a digital clock recovery loop was later implemented on the FPGA and then tested to estimate the power consumption of the digital back-end in a system implementation.

To measure the gain of the analog receiver ($v_{\mathrm{in,ADC}}/v_{\mathrm{in,LNA}}$) across frequency, an OOK-modulated current signal was applied at the receiver input ($i_S' = 2.25\ \mathrm{nA_{rms}}$) and the baseband output ($v_{\mathrm{in,ADC}}$) was measured as the carrier frequency was swept. The measurements were done for different gain settings of the first and the second stage VGAs using bits g[0:1] and g[2:3]. The maximum measured gain (for gain setting 0000) is 56 dB at 40.6 kHz (Fig. 17). Since the two VGA stages are identical, similar gains are measured for settings 0001 and 0100, and for 0010 and 1000. The measured receiver bandwidth is 2.6 kHz and is limited by the bandwidth of the resonance peaking circuit.

To measure the BER characteristics, the amplitude of the OOK signal at the LNA input ($v_{\mathrm{in,LNA}}$) was changed by tuning the attenuator and the corresponding BER values were measured; Fig. 18 shows the measured BER curve. At a data rate of 250 bps, the receiver sensitivity ($\mathrm{BER} = 10^{-3}$) is 19 $\mu\mathrm{V_{rms}}$ for a receiver power consumption of 4.4 μW. Thus, the targeted receiver sensitivity, as derived in Section II.F, was achieved. For higher data rates, filtering from the resonance peaking network resulted in degradation in sensitivity. Table I summarizes the electrical-only performance of the receiver.

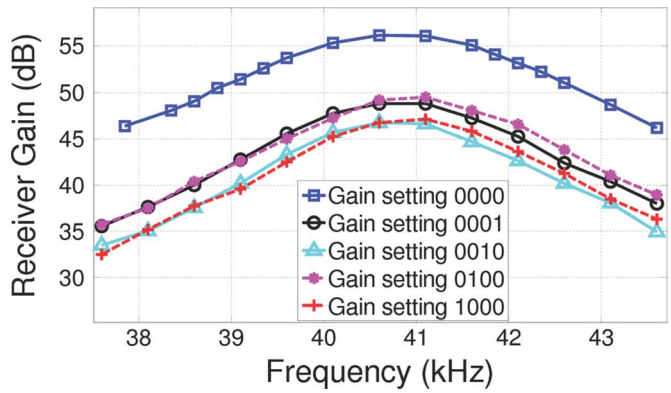

Fig. 17. Measured receiver gain ($v_{in,ADC}/v_{\mathrm{in,LNA}}$) vs. frequency for different gain settings for an input voltage signal ($v_{\mathrm{in,LNA}}$) of 80 μV_{rms}.

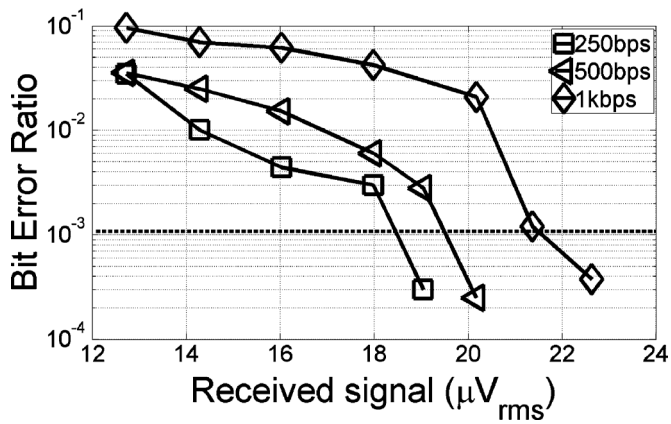

Fig. 18. BER plots for an electrical input signal.

B. In-Field Measurements for the Ultrasound Data Link

The communication distance range was estimated by combining the electrical-only RX chip BER measurements (Fig. 18), the pressure-distance in-field measurements (Fig. 6)

TABLE I
RECEIVER PERFORMANCE SUMMARY

Ultrasonic Carrier Frequency	40.6 kHz
Modulation	OOK
Supply Voltage	0.6 V
IC Technology	CMOS65nm
Chip area (including bondpads)	1.24 mm^2
Package	QFP64
Power Consumption	
Low Noise Amplifier	1.62 µW
Carrier-band VGA and filter	0.72 µW
Squarer and baseband amplifiers	1 µW
Biasing	0.66 µW
5-bit ADC 2 kS/s	400 nW
Total Receiver	4.4 µW
Measured electrical-only receiver sensitivity for BER < 10^{-3}	< 20 μV_{rms}
Measured distance range in free-space (lecture hall) with -18-dBm power into the TX transducer with BER < 10^{-3}	> 8.6 m

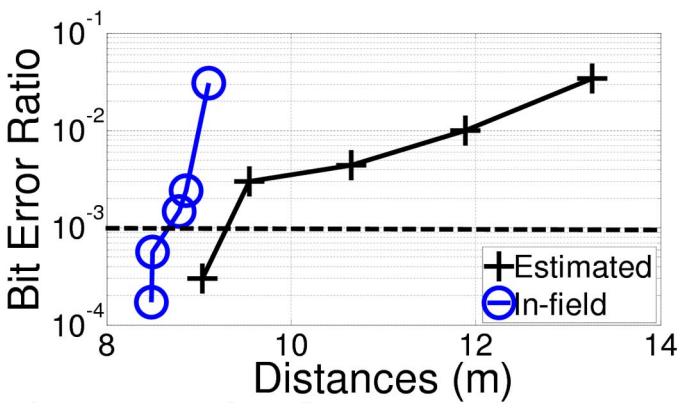

Fig. 19. The estimated communication distance range obtained by combining the electrical and mechanical characterization curves, and the BER vs. distance curve for a 250 bps random data signal measured in free space in a lecture hall.

and the TX-RX pair transmission characteristics (Fig. 5). Fig. 19 shows the estimated distance ranges.

To measure the receiver performance in a real environment, a through-air wireless ultrasound communication system was set up in a lecture hall. The ultrasonic transmitter was constructed with the commercial ultrasonic transmit transducer [17], a cyclone II FPGA to generate transmit data bits, a sine-wave generator, and a discrete mixer. The random bits at a rate of 250 bps are mixed with the 40.6-kHz carrier wave to generate an OOK voltage signal, that excites the transmit transducer.

For a fixed value of transmit power, the transmitter-receiver distance is changed and the BER values are measured. A BER lower than 10^{-3} and a data rate of 250 bps could be achieved for a TX-RX distance of 8.6 m, when the transmitter was excited with an electrical signal of power 16 μW (-18 dBm) (Fig. 19). The communication distance range matches well with the estimated values. The nature of the measured and the estimated curves are different because the method of estimating the distance range does not take into account the finite bandwidth of the transducer pair, however it provides a simple and an intuitive approach. The in-field BER was limited by the circuit noise, though some effect of reverberations has also been observed when the receiver was placed near the edges of the room.

V. DISCUSSION

Table II compares the performance of the presented wake-up receiver to the state-of-the-art wake-up receivers. We note the very low power dissipation of the presented ultra-sound solution thanks to the low carrier frequency that the receiver needs to process compared to RF based solutions. In addition the following references target low power wake-up receiver designs. In [26], correlation functions have been realized in the baseband to achieve an ultra-low power consumption of 2.4 μW. However, the authors claim a sensitivity of -71 dBm, but define it using a different criterion than the usual bit-error-ratio; the sensitivity has been presented in terms of the probabilities of missed detection and false alarm for a 64-bit wake-up[5]. In [27], authors claim a power consumption of 11 μW by using error correction coding in the digital baseband; however, the sensitivity is very poor at -57 dBm. Paper [28] presents a nanowatt wake-up receiver. However, the distance range for this system is only 2 m and the sensitivity of this receiver does not suffice for an application like wireless sensor networks. A 8.7 μW wake-up receiver has been presented in [29] for underwater communication. However, at 100 $\mu V_{\rm rms}$, the sensitivity of the receiver is too low for over-the-air communication.

VI. CONCLUSION

The paper presents a 4.4-μW ultrasonic wake-up receiver IC designed in a 65-nm CMOS process. Unlike a duty-cycled main receiver for which the figure-of-merit is energy/bit, the wake-up receiver is always ON and the key design criterion is continuous power consumption. Ultrasound enables ultra-low power wake-up by facilitating much lower circuit speeds; the centimeter-scale wavelengths of ultrasonic waves enables small-size transducers even for frequencies as low as a few tens of kilohertz. The 40-kHz ultrasound wake-up receiver IC demonstrated in this research has been electrically characterized and then tested in field; it achieves communication distance ranges targeted by WSN applications. Additionally, the power being put into the transmitter transducer is approximately 18 dB lower than the typical values used in RF links. Table II summarizes the performance comparisons of the comparable state-of-the-art wake-up receivers.

ACKNOWLEDGMENT

The authors would like to thank Shih-An Yu, Jayanth Kuppambatti, Chunwei Hsu, Nadia Pervez, and Prof. Mingoo Seok, all with Columbia University, for technical insights

[5]This way of defining sensitivity makes comparison with other wake-up receivers very hard, because with a 64-bit wake-up packet, probabilities of missed detection and false alarm of less than 0.15% can be achieved even with relatively high bit error rates of around 0.1. It should be noted that for a BER of 10^{-3}, as achieved in this work, a 20-bit wake-up pattern suffices to keep probabilities of both missed detection and false alarm below 0.1.

TABLE II
PERFORMANCE COMPARISON

	Carrier	LOS or NLOS	Path-loss exponent (n)	Data Rate	Transmit Signal Power (Transmit energy per bit)	RX power consumption	Communication Distance
[4]	Infra-red (38kHz)	LOS	-	500-1kbps	110 mW (110 μJ-220 μJ)	286 μW	10 m[a]
[6]	RF (2 GHz)	NLOS	3	10-100 kpbs	1 mW[b] (10nJ-100nJ)	52 μW	13 m[c]
[7]	RF (2.4 GHz)	NLOS	3	10-100 kbps	1 mW[b] (10nJ-100nJ)	51 μW	10.5 m[d]
This Work	Ultrasound (40 kHz)	LOS	2.2	250 bps	16 mW (64 nJ)	4.4 μW	8.6 m[a]

[a] Measured in-field distance range.

[b] Assuming a path-loss exponent of n=2.2, transmit signal powers of 52 μW and 98 μW will be needed for [6] and [7] to achieve the same distance range (8.6 m) as that of the ultrasonic wake-up receiver presented in this work.

[c] Estimated distance range as presented in [30] with isotropic and lossless transmit and receive antennas.

[d] Estimated distance range using the exponent from [30] and assuming both the transmit and receive antennas to be both lossless and isotropic.

and discussions. The authors would also like to acknowledge Mediatek for chip fabrication donation.

REFERENCES

[1] B. W. Cook, S. Lanzisera, and K. S. J. Pister, "SoC issues for RF smart dust," *Proc. IEEE*, vol. 94, pp. 1177–1196, Jun. 2006.

[2] E.-Y. Lin, J. Rabaey, and A. Wolisz, "Power-efficient rendezvous schemes for dense wireless sensor networks," in *Proc. IEEE Int. Conf. Communications*, Jun. 2004, vol. 7, pp. 3769–3776.

[3] E.-Y. Lin, "A Comprehensive Study of Power-Efficient Rendezvous Schemes for Wireless Sensor Networks," Ph.D. dissertation, Dept. Elect. Eng., Univ. of California, Berkeley, CA, 2005.

[4] H. Ishihara *et al.*, "A 130-μA wake-up receiver SoC in 0.13-μm CMOS for reducing standby power of an electric appliance controlled by an infrared remote controller," in *IEEE Int. Solid-State Circuits Conf. Dig.*, Feb. 2011, pp. 226–228.

[5] K. Yadav, I. Kymissis, and P. Kinget, "A 4.4-μW wake-up receiver using ultrasound data communication," in *VLSI Circuits Symp. Dig.*, Jun. 15–17, 2011, pp. 212–213.

[6] N. M. Pletcher, S. Gambini, and J. Rabaey, "A 52-μW wake-up receiver with −72-dBm sensitivity using an uncertain-IF architecture," in *IEEE Int. Solid-State Circuits Conf. Dig.*, Feb. 2008, pp. 524–633.

[7] X. Huang, S. Rampu, X. Wang, G. Dolmans, and H. de Groot, "A 2.4 GHz/915 MHz 51-μW wake-up receiver with offset and noise suppression," in *IEEE Int. Solid-State Circuits Conf. Dig.*, Feb. 2010, pp. 222–223.

[8] Y. Zhang, L. Huang, G. Dolmans, and H. de Groot, "An analytical model for energy efficiency analysis of different wakeup radio schemes," *Personal, Indoor and Mobile Radio Communications*, pp. 1148–1152, Sep. 2009.

[9] K. Martinez, J. K. Hart, and R. Ong, "Environmental sensor networks," *IEEE Computer*, vol. 37, pp. 50–56, Aug. 2004.

[10] "P-tag datasheet," [Online]. Available: http://www.sonitor.com/technology/tags/p-tag

[11] H. E. Bass and L. N. Bolen, "Ultrasonic background noise in industrial environments," *J. Acoust. Soc. Am.*, vol. 78, no. 6, pp. 2013–2016, Dec. 1985.

[12] S. Holm, "Airborne ultrasound data communications: The core of an indoor positioning system," in *Proc. IEEE Int. Ultrasonics Symp.*, Sept. 2005, vol. 3, pp. 1801–1804.

[13] D. Goldberg, A. Andreou, P. Julian, P. Pouliquen, L. Riddle, and R. Rosasco, "A wake-up detector for an acoustic surveillance sensor network: Algorithm and VLSI implementation," in *Int. Symp. Information Processing in Sensor Networks*, 2004.

[14] U. S. Food and Drug Administration, "Information for manufacturers seeking marketing clearance of diagnostic ultrasonic systems and transducers," [Online]. Available: http://www.fda.gov Sep. 9, 2008

[15] *Occupational Safety and Health Standards*, 1910.95, Occupation Safety and Health Administration, U.S. Dept. of Labor [Online]. Available: http://www.osha.gov

[16] American Conference of Governmental Industrial Hygienists, "Threshold limit values for chemical substances and physical agents and biological exposure indices," 2002 [Online]. Available: http://www.acgih.org

[17] "40 kHz transmit (40KT25) senscomp," [Online]. Available: http://www.senscomp.com/pdfs/k-series-40kt25- 40kr25.pdf

[18] "40 kHz receive (US40KR/US40KT)," [Online]. Available: http://www.ehag.ch/PDFFiles/ MSI/40khz_receiver.pdf

[19] "Models and parameters of piezoelectric transducers," in *The Applications of Ferroelectric Polymers*, T. T. Wang, J. M. Herbert, and A. M. Glass, Eds. New York: Chapman and Hall, 1988.

[20] Z. Chang and W. M. C. Sansen, "Low-noise, low-distortion CMOS AM wide-band amplifiers matching a capacitive source," *IEEE J. Solid-State Circuits*, vol. 25, no. 3, pp. 833–840, Jun. 1990.

[21] "Microphone, preamplifier (377C01,426B03)," [Online]. Available: http://www.pcb.com/spec_sheet.asp?model=377C01,http://www.pcb.com/spec_sheet.asp?model=426B03

[22] D. R. Griffin, "The importance of atmospheric attenuation for the echolocation of bats (Chiroptera)," *Animal Behavior*, vol. 19, pp. 55–61, Feb. 1971.

[23] D. A. Johns and K. Martin, *Analog Integrated Circuit Design*, 1st ed. New York: Wiley, 1997.

[24] P. Zicari, P. Corsonello, and S. Perris, "A high flexible early-late gate bit synchronizer in FPGA-based software defined radios," in *Proc. 4th Eur. Conf. Circuits and Systems for Communications*, Jul. 2008, pp. 252–255.

[25] I. Kuon and J. Rose, "Measuring the gap between FPGAs and ASICs," in *Proc. ACM/SIGDA 10th Int. Symp. Field-Programmable Gate Arrays*, 2006, pp. 21–30.

[26] C. Hambeck, S. Mahlknecht, and T. Herndl, "A 2.4-μW wake-up receiver for wireless sensor nodes with −71-dBm sensitivity," in *Proc. IEEE Int. Symp. Circuits and Systems*, May 2011, pp. 534–537.

[27] M. Spinola-Durante and S. Mahlknecht, "An ultra low power wakeup receiver for wireless sensor nodes," in *Proc. Int. Conf. Sensor Technologies and Applications*, Jun. 2009, pp. 167–170.

[28] S. J. Marinkovic and E. M. Popovici, "Nano-power wireless wake-up receiver with serial peripheral interface," *IEEE J. Sel. Areas Commun.*, vol. 29, pp. 1641–1647, Sep. 2011.

[29] A. Sanchez, S. Blanc, P. Yuste, and J. J. Serrano, "RFID based acoustic wake-up system for underwater sensor networks," in *Proc. IEEE 8th Int. Conf. Mobile Adhoc and Sensor Systems*, Oct. 2011, pp. 873–878.

[30] N. Pletcher, "Ultra-Low Power Wake-Up Receivers for Wireless Sensor Networks," Ph.D. dissertation, Dept. Elect. Eng, Univ. of California, Berkeley, CA, May 2008.

Kshitij Yadav (S'13) received the B.Tech. and M.Tech. degrees in electronics and electrical communication engineering from Indian Institute of Technology (IIT) Kharagpur, India, in 2007. He received the Ph.D. degree in electrical engineering from Columbia University, New York, in October 2012. His research has been focused on design of ultrasound pressure sensors and accompanying electronics for ultrasound data communication.

He has done summer internships at Linear Technology, North Chelmsford, MA, and at Alcatel-Lucent Bell Labs, Murray Hill, NJ. He has also been a visiting scholar at the University of California, Santa Cruz and at Texas A&M University. He co-founded the company Udacomm Inc. for commercializing through-air ultra-low-power wireless-ultrasound communication in July 2012 and is currently a Principal Investigator on a Phase I National Science Foundation (NSF) Small Business Innovation Research (SBIR) Grant through which Udacomm is being funded July 2012–Dec 2012. He was also the leader of the team that won the $100K first prize in the 2012 Interdigital Wireless Innovation Challenge (I2C).

Ioannis Kymissis (M'03–SM'10) received the S.B., M.Eng., and Ph.D. degrees in electrical engineering and computer science from the Massachusetts Institute of Technology (MIT), Cambridge, MA, in 1998, 1999, and 2003, respectively.

After graduation he served as a postdoctoral associate at MIT and as a consulting senior engineer at QDVision, which is commercializing quantum dot-based photoluminescent and electroluminescent systems. He joined the faculty of Electrical Engineering of Columbia University, New York, in 2006, where he now serves as an Associate Professor. His research interests include the application of organic field-effect transistors (FETs) to large-area-compatible sensing and actuation systems and the application of thin-film technology to sensing, display, energy conversion, and large-area actuators.

He was the recipient of the IEEE EDS Paul Rappaport Award in 2002 for his contributions to organic FET technology, the Shoulders Grey Spindt award at the 2002 International Vacuum Microelectronics Conference for his contributions to vacuum microelectronics, the National Science Foundation Faculty Early Career Development (CAREER) Award in 2006, the 2011 IEEE Communications Society Award for Advances in Communications, and the First Prize ($100K) in the 2012 Interdigital Wireless Innovation Challenge (I2C). He also currently serves as the editor in chief of the Journal of the Society for Information Display.

Peter R. Kinget (M'90–SM'02–F'11) received the engineering degree (*summa cum laude*) in electrical and mechanical engineering and the Ph.D. (*summa cum laude* with Congratulations of the Jury) in electrical engineering from the Katholieke Universiteit Leuven, Belgium, in 1990 and 1996, respectively.

From 1991 to 1995, he received a graduate fellowship from the Belgian National Fund for Scientific Research (NFWO) and was a Research Assistant at the ESAT-MICAS Laboratory of the Katholieke Universiteit Leuven. From 1996 to 1999 he was at Bell Laboratories, Lucent Technologies, in Murray Hill, NJ, as a Member of Technical Staff in the Design Principles Department. From 1999 to 2002 he held various technical and management positions in IC design and development at Broadcom, CeLight and MultiLink. In 2002 he joined the faculty of the Department of Electrical Engineering, Columbia University, NY. During 2010–2011, he was at the Université catholique de Louvain, Belgium, on sabbatical leave. He also serves as an expert on patent litigation and a technical consultant to industry. His research interests are in analog, RF and power integrated circuits and the applications they enable in communications, sensing, and power management. He is widely published in circuits and systems journals and conferences, has co-authored 3 books and holds 11 US patents with several applications under review. His research group has received funding from the National Science Foundation, the Semiconductor Research Corporation, the Department of Energy (ARPA-E), the Department of Defense (DARPA), and an IBM Faculty Award. It has further received in-kind and grant support from several of the major semiconductor companies.

Dr. Kinget is a Fellow of the IEEE. He is an elected member of the IEEE Solid-State Circuits Adcom (2011–2013). He has been an IEEE Distinguished Lecturer of the Solid-State Circuits Society (2009–2010) and an Associate Editor of the IEEE JOURNAL OF SOLID-STATE CIRCUITS (2003–2007) and the IEEE TRANSACTIONS ON CIRCUITS AND SYSTEMS II (2008–2009). He has served as a member of the Technical Program Committee of the IEEE Custom Integrated Circuits Conference (2000–2005), the Symposium on VLSI Circuits (2003–2006), the European Solid-State Circuits Conference (2005–2010) and the IEEE International Solid-State Circuits Conference (2005–2012). He is a co-recipient of several awards including the Best Student Paper Award–1st Place at the 2008 IEEE Radio Frequency Integrated Circuits (RFIC) Symposium, the First Prize in the 2009 Vodafone Americas Foundation Wireless Innovation Challenge, the Best Student Demo Award at the 2011 ACM Conference on Embedded Networked Sensor Systems (ACM SenSys), the 2011 IEEE Communications Society Award for Advances in Communications, and the First Prize ($100K) in the 2012 Interdigital Wireless Innovation Challenge (I2C).